

NOVEL CARRAGEENAN/REDUCED GRAPHENE OXIDE/Ag COMPOSITE AS ADSORBENT FOR REMOVAL METHYLENE BLUE FROM AQUEOUS SOLUTION

Y. ZHENG^{a,b}, J. YANG^a, R. YANG^a, A. WANG^c, B. DENG^b, F. PENG^a,
Y. PENG^d, L. HE^c, L. FU^{a*}

^a*Institute of Botany, Jiangsu Province and Chinese Academy of Sciences, Nanjing Botanical Garden, Mem. Sun Yat-Sen, Nanjing 210014, China*

^b*Jiangsu Junma Park Technology Co. Ltd, Jiangsu, China*

^c*Department of Physics and Materials Science, City University of Hong Kong, Hong Kong*

^d*College of Forestry and Biotechnology, Zhejiang Agriculture and Forestry University, Lin'an, Zhejiang, China*

^e*Beijing Petrochemical Engineering Corp. LTD, Chaoyang District Tianjuyuan Building No. 7, Beijing, China*

Carrageenan/reduced graphene oxide/Ag composite (CA/RGO/Ag) was synthesized by a wet chemical method at room temperature using carrageenan, graphene oxide and silver nitrate as starting materials. As-prepared composite was characterized by UV-vis spectroscopy, FTIR, SEM, and XRD. Results showed that the reduction of graphene oxide (GO) and silver nitrate was achieved simultaneously by addition of NaBH₄. CA/RGO/Ag composite was used for adsorption of methylene blue (MB) from aqueous solution. The effect of parameters such as the ratio of GO and silver nitrate, contact time, pH, temperature, and mass of the composite has been investigated. The adsorption isotherm data could be well explained by Langmuir isotherm model. According to our results, the CA/RGO/Ag composite is a suitable adsorbent candidate for purifying of water pollution.

(Received January 12, 2015; Accepted April 10, 2015)

Keyword: Carrageenan; Reduced graphene oxide; Silver; Adsorption; Methylene blue

1. Introduction

Dyes are widely used in numerous industries such as textile, paper, food, light-harvesting arrays, cosmetics and pharmaceuticals. Most of them are serious threats to the environment and human health because they can be stabilized, remaining in the water for a long time [1]. According to the report, 280,000 tons of dye materials enter directly into effluents around the world annually [2]. Therefore, development of dye removal technique is crucial for environment protection as well as human health. Technologies like photodegradation, precipitation, membrane separation, amalgamation and ion-exchange was developed for removing dye pollutant from water [3-8]. Among these techniques, adsorption process is noted to be superior to other methods due to its economically cost effective, high flexibility, easy automation and simple operation process [9-14].

The selection of adsorbent is essential for adsorption processes. Usually, a good adsorbent candidate should meet three standards: high specific surface area, pore volume accessible for the adsorbate molecules and easy regeneration. Recently, using graphene as an adsorbent to solving environmental pollution problems has received considerable attention due to its high specific surface area and unique 2D structure for composite material designing. Several theoretical calculations and experimental measurements were conducted for using graphene as an adsorbent to remove hazardous pollutants from aqueous solutions [15-19]. Recent literature suggests that

*Corresponding author: lifu@swin.edu.au

graphene based composites showed excellent performances for hazardous pollutants removal. For example, Sreepasad et al. [20] synthesized a reduced graphene oxide (RGO)-MnO₂ composites for removing Hg(II) from water. The composites showed enhanced removal capability compared to the parent material. However, the graphene used for composite design usually in its reduced form from graphene oxide (GO) prepared by the oxidation of graphite. The RGO naturally has a tendency to agglomerate irreversibly, or even to restack into graphite through Van der Waals interactions [21-23]. Therefore, surface functionalization is considered as an effective way to solve this problem. In this report. We explore the possibility of using carrageenan functionalized RGO/Ag (CG/RGO/Ag) composite for removal of methylene blue from aqueous solution. The synthesized composites were also characterized by UV-vis spectroscopy, SEM, XRD and FTIR.

2. Experimental

2.1 Materials

Synthetic graphite (average particle diameter <20 μm), silver nitrate (AgNO₃), carrageenan, methylene blue (MB) and sodium borohydrid (NaBH₄) were purchased from Sigma-Aldrich. All other chemicals used were analytical grade reagents without further purification. Milli-Q water (18.2 MΩ cm) was used throughout the experiments.

2.2 Synthesis of CG/RGO/Ag composite

Graphene oxide was prepared using modified Hummer's method [24, 25]. In a typical procedure, 125 ml of concentrated sulfuric acid was taken into a flask filled with graphite powder (5 g) followed by the addition of KMnO₄ (17.5 g) slowly at 0 °C. The mixture was stirred for 3 h at 35 °C and then diluted by water at 0 °C. After that, H₂O₂ (30 vol.% in water) was added into mixture until the bubbling of the gas was completed. The graphene oxide (GO) powder was collected by centrifugation of the solution and subsequently dried under vacuum at 80°C for 24 h.

To synthesize CG/RGO/Ag composite, 0.5 mg carrageenan was dissolved into 50 mL water by 30 min sonication to form a brown solution. 10 mL GO dispersion (1 mg/mL) was added into carrageenan solution for 1 h stirring. After that, a certain amount of AgNO₃ solution (50 mM) was added into the mixture for another hour stirring. Then, 1 mL NaBH₄ solution (0.5 M) was added to the above mixture dropwise. The color of the mixture turned from brown to black. After 30 min stirring, the composite was centrifuged, washed and dried at 80°C for 24 h. (denoted as CG/RGO/Ag-1, CG/RGO/Ag-2, CG/RGO/Ag-3, CG/RGO/Ag-4, CG/RGO/Ag-5 and CG/RGO/Ag-6 for the weight ratios of GO and AgNO₃ set as 1:5, 1:10, 1:20, 1:30, 1:40 and 1:50, respectively). CG/RGO and RGO/Ag sample also synthesized using a similar method except addition of AgNO₃ and carrageenan, respectively.

2.3 Characterizations

Surface morphology of samples were analyzed by scanning electron microscope (SEM, S-4700, HITACHI). FTIR spectra were obtained using a Nicolet 8700 FTIR spectrometer (Thermo Scientific Instrument). X-ray diffraction patterns were collected from 10° to 60° in 2θ by a XRD with Cu Kα radiation (D8-Advanced, Bruker).

2.4 MB adsorption experiments

To investigate the adsorption capability of the adsorbents, the MB was selected as the model dye. The experiments were carried out by putting a certain weight of adsorbent into 50 mL MB aqueous solution. The dye solution was magnetically stirred over the magnetic stirring rod throughout the experiment. At a specified time interval, 1.5 mL of suspension was then taken out, separated by centrifugation. The absorption of MB was then measured by a UV-vis spectroscopy. The absorbance of MB at 664 nm was used for measuring the concentration change. The uptake amount of dye molecules was calculated by the following equation:

$$q_t = \frac{C_0 - C_e}{m} \times V$$

Where m is the mass of adsorbent in g, V is the volume of MB solutions in L and C_0 and C_e are the initial and equilibrium concentrations in mg/L, respectively.

3. Results and discussion

The formation of Ag nanoparticles and reduction of GO was confirmed by UV-vis spectroscopy. Fig. 1A shows the UV-vis spectra of GO and CA/RGO-Ag composite. The spectrum of GO displays a maximum absorption peak centered at 228 nm and a shoulder peak at about 316 nm, corresponding to $\pi-\pi^*$ transitions of aromatic C—C bonds and $n-\pi^*$ transitions of C=O bonds [26]. In the spectrum of CA/RGO-Ag-6 composite, the absorption peak of GO dispersion at 228 nm gradually red-shifted to 242 nm and the shoulder absorption peak at 316 nm disappeared, indicating that the GO has been reduced by NaBH_4 . Moreover, a new peak at 421 nm is also observed in the spectrum of CA/RGO-Ag-6 composite, which related to the surface plasmon resonance absorption band of Ag nanoparticles, indicating the formation of Ag nanoparticles.

The surface functionalization process was confirmed by the FTIR study. Fig. 1B shows the FTIR spectra of GO, carrageenan and CA/RGO-Ag-6 composite. As expected, the spectrum of GO exhibits signals at 3432, 1638, 1156 and 1038 cm^{-1} corresponding to the —OH vibration stretching, carboxyl C=O, epoxy C—O and alkoxy C—O, respectively [27]. It can be seen that these peaks show a relatively lower intensity or even vanished in the spectrum of CA/RGO-Ag-6 composite, further confirm the reduction of GO. The spectrum of carrageenan shows the peaks at 2900 and 1374 cm^{-1} , which can be assigned as the vibration of C—O bonds. Moreover, the spectrum also exhibits three characteristic peaks for carrageenan at 1225, 915 and 852 cm^{-1} [28, 29]. These peaks also were observed in the spectrum of CA/RGO-Ag-6 composite, indicating the successful surface functionalization of carrageenan.

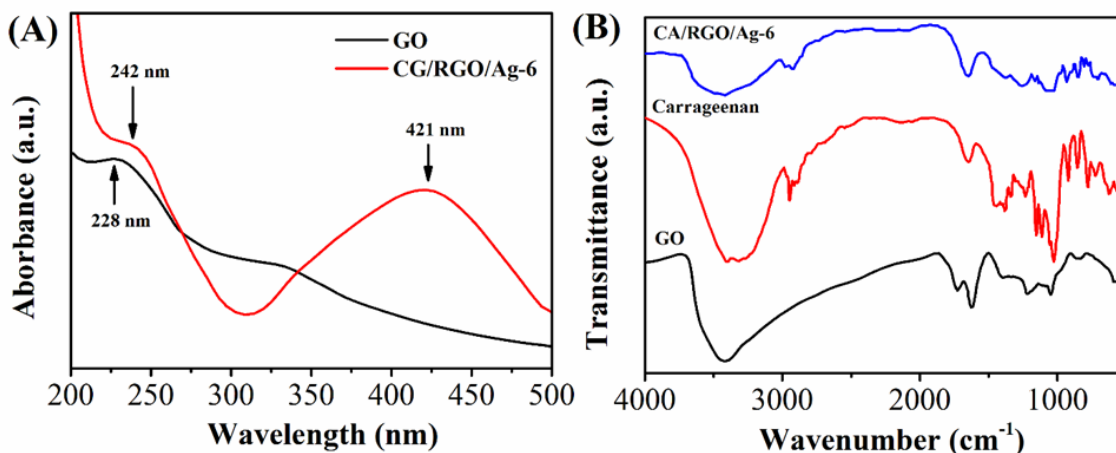


Fig. 1. (A): UV-vis spectra of GO and CA/RGO/Ag-6. (B): FTIR spectra of GO, carrageenan and CA/RGO/Ag-6.

Fig. 2 shows the morphology of as-prepared RGO/Ag, CA/RGO-Ag-1, CA/RGO-Ag-3 and CA/RGO-Ag-6 composite. Compared with CA/RGO-Ag composite, RGO/Ag exhibits a completely different morphology, Ag nanoparticles show an aggregated cluster form and touch on the RGO sheet surface. However, in the CA/RGO-Ag composite, RGO sheets are embedded into carrageenan gel. On the composite surface, we could observe a uniform distribution of single Ag nanoparticles when a higher AgNO_3 content was introduced during the preparation.

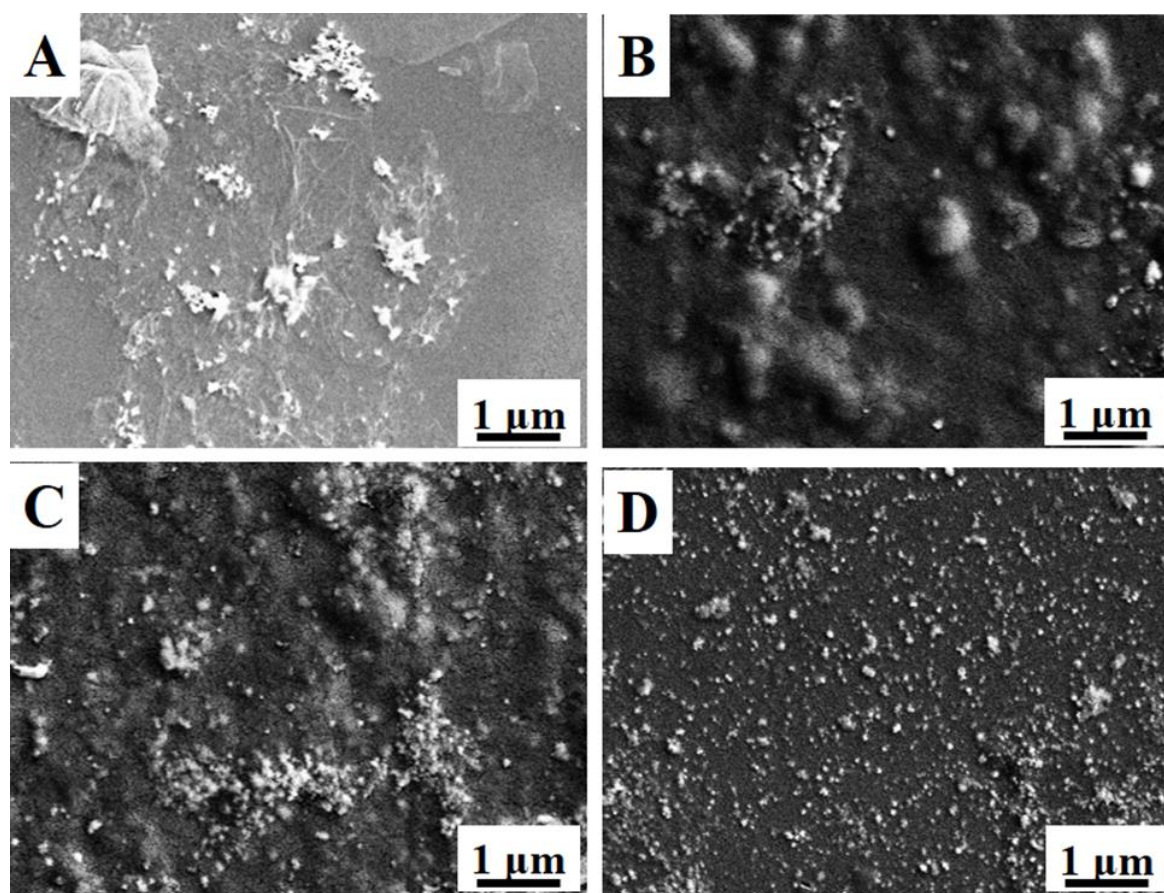


Fig. 2. SEM images of (A) RGO/Ag, (B) CA/RGO/Ag-1, (C) CA/RGO/Ag-3 and (D) CA/RGO/Ag-6.

The powder X-ray diffraction of the samples are shown in Fig. 3. The diffraction pattern of the GO displays a characteristic peak at 11.2° . This peak is not seen for CA/RGO/Ag-6 composite, further indicating the GO has been reduced. The crystallinity of carrageenan is depends on the oriented packing of helices, however, there is no obvious peaks can be observed in the CA/RGO/Ag-6 composite, indicating the carrageenan lost its crystallinity after interaction with GO and Ag nanoparticles. Moreover, the presence of diffraction peak at 38.4° and 44.7° can be assigned to the (111) and (200) lattice planes of the Ag nanoparticles, respectively [30].

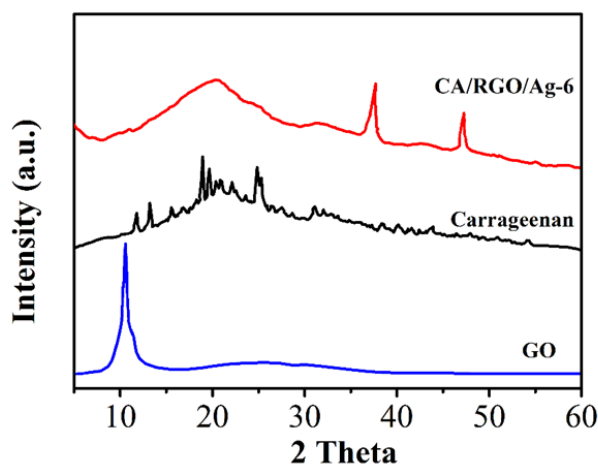


Fig. 3. XRD patterns of GO, carrageenan and CA/RGO/Ag-6.

Fig. 4 shows the adsorption rate of MB (1×10^{-5} M) on 20 mg of CA/RGO/Ag -1, CA/RGO/Ag -2, CA/RGO/Ag -3, CA/RGO/Ag -4, CA/RGO/Ag -5, CA/RGO/Ag -6 and RGO/Ag composite. It can be seen that all CA/RGO/Ag composites show superior absorption property than that of RGO/Ag composite, indicating the incorporation of carrageenan could highly increase the adsorption capacity of adsorbent. The CA/RGO/Ag-4 composite exhibits the best adsorption capacity, which could remove almost all of the MB molecules in the aqueous system. Therefore, the weight ratio of GO and AgNO₃ for fabricating CA/RGO/Ag adsorbent was set as 1: 30. The high percentage removal of MB by CA/RGO/Ag composite can be attributed to the high specific surface area of carrageenan functionalized RGO sheets and the catalytic activity of the surface deposited Ag nanoparticles [31, 32]. Moreover, the RGO/Ag composite could reach to adsorption equilibrium within 20 min, while the CA/RGO/Ag composites require about 35 min, suggesting the incorporation of carrageenan may decrease the surface adsorption rate.

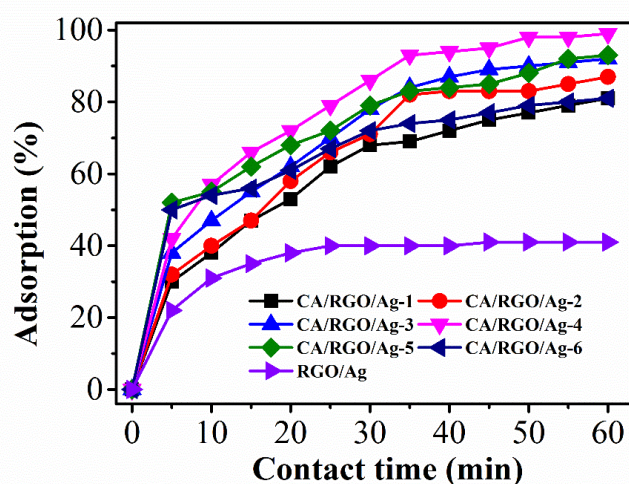


Fig. 4. Adsorption profiles of MB on CA/RGO/Ag -1, CA/RGO/Ag -2, CA/RGO/Ag -3, CA/RGO/Ag -4, CA/RGO/Ag -5, CA/RGO/Ag -6 and RGO/Ag composite.

The effect of temperature on adsorption was investigated using 50 mL MB (1×10^{-5} M) on 20 mg of CA/RGO/Ag -4. The results are shown in Fig. 5A. It can be observed that the adsorption capacity of CA/RGO/Ag -4 increases with temperature rise. It because the adsorption of MB is an endothermic process. In this study, the highest value of q_e was reached 39.72 mg/g with a removal rate of 99.7% at 340 K.

Generally, waste water released from industries possesses a wide range of pH. Therefore, the pH of the system is very important parameter on the adsorption process. Fig. 5B displays the effect of pH on the adsorption of MB onto CA/RGO/Ag -4 composite. It can be seen that increasing the pH from 2 to 9, adsorption capacity of CA/RGO/Ag -4 composite is increased from 30.51 to 38.12 mg/g. Further increasing the pH to 12, result no change in the adsorption capacity. The possible explanation of high adsorption performance at high pH condition could be the change of the surface charge. At higher pH condition, the surface of CA/RGO/Ag -4 composite becomes predominate negative charge, which could adsorb more cationic MB molecules. Similarly several researchers have demonstrated the same result in which adsorption capacity of adsorbent was increased with increase in the pH of MB solution [33, 34].

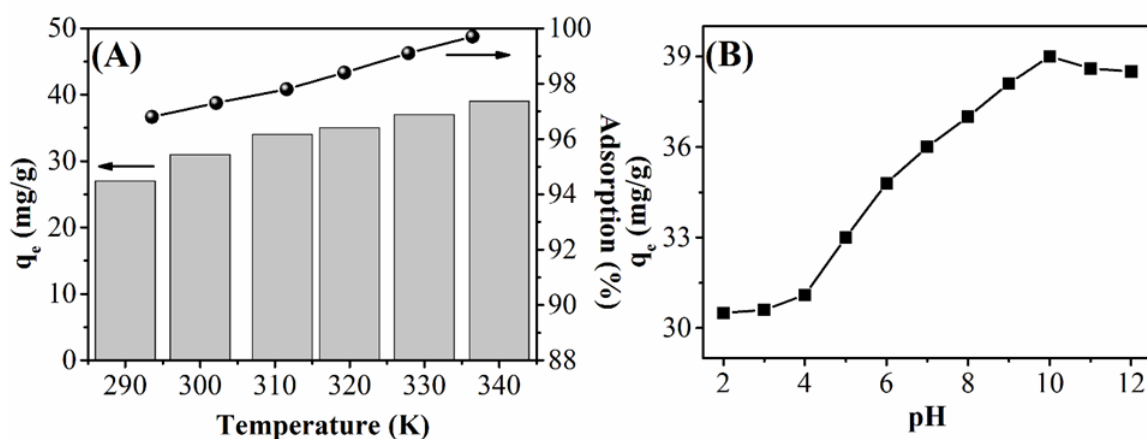


Fig. 5. (A) Effect of temperature and (B) effect of pH on preferential adsorption of MB dye on CA/RGO/Ag-4.

The effect of adsorbent content on adsorption of MB was also studied. A series of adsorption experiments were conducted with varied amount of CA/RGO/Ag-4 (5–50 mg) and 50 mL of MB solutions (1×10^{-5} M). The results indicate that increasing the CA/RGO/Ag-4 dosage from 5 mg to 20 mg, the adsorption performance of CA/RGO/Ag-4 increases from 28.28 mg/g to 39.87 mg/g (Fig. 6A). Simultaneously the removal rate of MB is increased from 23.54% to 97.7% respectively. However, further increase in the amount of CA/RGO/Ag-4 from 20 mg to 50 mg, the adsorption capacity of CA/RGO/Ag-4 for MB is decreased to 17.25 mg/g. Therefore 20 mg of adsorbent was optimized for this work.

In order to investigate the effect of initial dye concentration on adsorption properties, a series of experiments were conducted using different concentration of MB solution with 20 mg of CA/RGO/Ag-4. As shown in Fig. 6B, the adsorption is very fast at lower initial concentration of MB solution. The percent removal of MB then decreases along with the increase in initial concentration of MB due to the fact that when the concentration increases, there will be increased competition for the active adsorption sites and the adsorption process will increasingly slow down [35].

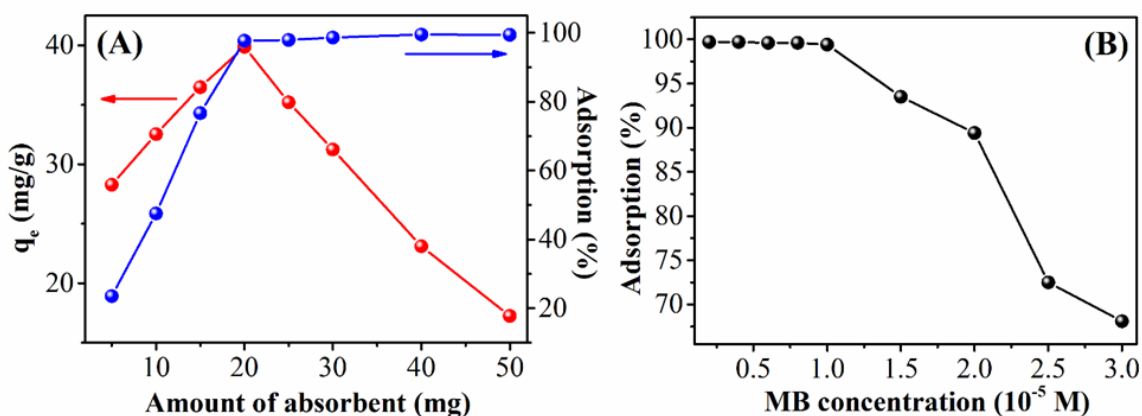


Fig. 6. (A) Effect of adsorbent dosage and (B) Effect of initial MB concentration on adsorption of MB using CA/RGO/Ag-4.

Adsorption isotherms are viable for describing the relationship between adsorbate molecules and the adsorbent surface and highlight the distribution of adsorbate molecules between the liquid and solid phases [36]. There are many methods for analyzing adsorption equilibrium

data. The equation parameters of these equilibrium models often provide some insight into the adsorption mechanism, the surface properties and affinity of the adsorbent for adsorbate [37, 38]. In this work, both Langmuir and Freundlich models are used to understand the experimental results.

The Langmuir isotherm model can be expressed by the linear form of following formula:

$$\frac{C_e}{q_e} = \frac{C_e}{q_{\max}} + \frac{1}{q_{\max} K_L} \quad (1)$$

Where q_e (mg/g) is the equilibrium amount of the MB adsorption by CA/RGO/Ag-4 composite, C_e (mg/L) is the MB concentration when equilibrium condition is reached. q_{\max} is (mg/g) is the maximum adsorption amount. K_L (L/mg) is the Langmuir constant related to the enthalpy of the process. The values of q_{\max} and K_L for adsorption of MB were calculated from the slope and intercept of the linear plot of C_e/q_e vs C_e . The linear plots are shown in Fig. 7 and results are summarized in Table 1.

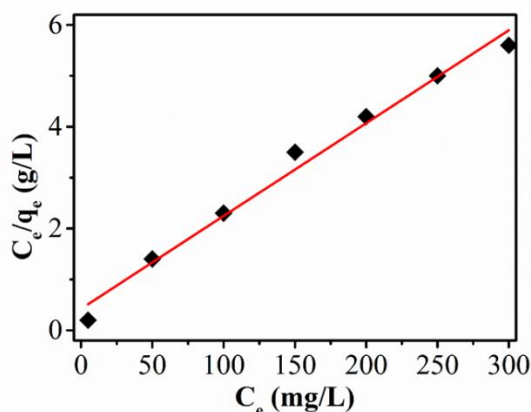


Fig. 7. Langmuir models of MB adsorption for CA/RGO/Ag -4.

The Freundlich isotherm model can be expressed by the linear form of following formula:

$$q_e = K_F C_e^{1/n} \quad (2)$$

Where K_F is the Freundlich constant related to the adsorption capacity of CA/RGO/Ag-4 composite. $1/n$ is the Freundlich exponent related to surface heterogeneity.

The logarithmic form of the Freundlich equation can be expressed as:

$$\log q_e = \log K_F + \frac{1}{n} \log C_e \quad (3)$$

The linear plots are shown in Fig. 8 and results are summarized in Table 1.

From the results, the MB adsorption on CA/RGO/Ag-4 is fitted into aforementioned two isotherm models. It can be seen that the result of the Langmuir isotherm model fit slightly better than the Freundlich model for preferential adsorption of MB. In summary, CA/RGO/Ag composite with relatively high adsorption capacity, rapid removal rate has great potential for industrial application in water treatment.

Table 1. Isotherm Constants of MB Adsorption for CA/RGO/Ag -4.

Isotherm model	Parameter	MB dye
Langmuir	q_{\max} (mg/g)	39.7
	K_L (L/mg)	0.02144
	R^2	0.997
Freundlich	K_F (mg/g)	32.41
	n	6.369
	R^2	0.988

4. Conclusion

The CA/RGO/Ag composite was successfully prepared via a facile wet chemical route. UV-vis and FTIR spectra confirmed the reduction of GO and formation of Ag nanoparticles. The as-prepared composite was used for removing MB dye from wastewater. The Langmuir isotherm is suitable for characterization experimental adsorption isotherm. Based on our results, the CA/RGO/Ag composite provides a simple and environment friendly separation method for the removal of dye pollutant from aqueous systems.

Acknowledgement

Authors acknowledge financial support from Jiangsu Planned Projects for Postdoctoral Research Funds (1402126C) and Jiangsu Planned Projects for Postdoctoral Research Funds (1402126C).

Reference

- [1] A. Duffy, G.M. Walker, S.J. Allen, *Chemical Engineering Journal* **117**, 239 (2006).
- [2] R. Maas, S. Chaudhari, *Process Biochemistry* **40**, 699 (2005).
- [3] T.S. Natarajan, H.C. Bajaj, R.J. Tayade, *Journal of colloid and interface science* **433**, 104 (2014).
- [4] C. Hachem, F. Bocquillon, O. Zahraa, M. Bouchy, *Dyes and Pigments* **49**, 117 (2001).
- [5] J. Wu, M. Eiteman, S. Law, *Journal of Environmental Engineering* **124**, 272 (1998).
- [6] G. Annadurai, R.-S. Juang, D.-J. Lee, *Advances in Environmental Research* **6**, 191 (2002).
- [7] L. Fu, W. Cai, A. Wang, Y. Zheng, *Materials Letters* **142**, 201 (2015).
- [8] S. Suresh, *Journal of Non-Oxide Glasses* **6**, 47 (2014).
- [9] M.R. Fathi, A. Asfaram, A. Farhangi, *Spectrochimica acta. Part A, Molecular and biomolecular spectroscopy* **135**, 364 (2015).
- [10] I. Pantic, *Reviews on Advanced Materials Science* **37**, 15 (2014).
- [11] L. Fu, Z. Fu, *Ceram Int* **41**, 2492 (2015).
- [12] E.S. Sazali, R. Sahar, S.K. Ghoshal, S. Rohani, R. Arifin, *Journal of Non-Oxide Glasses* **6**, 61 (2014).
- [13] C.P. Ganea, L. Frunza, I. Zgura, N. Preda, E. Matel, S. Frunza, *Digest Journal of Nanomaterials and Biostructures* **9**, 1493 (2014).
- [14] M.M. Byranvand, A.N. Kharat, *Journal of Ovonic Research* **10**, 191 (2014).
- [15] J. Björk, F. Hanke, C.-A. Palma, P. Samori, M. Cecchini, M. Persson, *The Journal of Physical Chemistry Letters* **1**, 3407 (2010).
- [16] G.K. Ramesha, A. Vijaya Kumara, H.B. Muralidhara, S. Sampath, *Journal of colloid and interface science* **361**, 270 (2011).
- [17] L. Liu, S. Liu, Q. Zhang, C. Li, C. Bao, X. Liu, P. Xiao, *Journal of Chemical & Engineering Data* **58**, 209 (2012).
- [18] L. Fu, Y. Zheng, Q. Ren, A. Wang, B. Deng, *Journal of Ovonic Research* **11**, 21 (2015).
- [19] N. Preda, M. Enculescu, A. Florica, A. costas, A. eEvangelidis, E. Matei, I. Enculescu, *Digest Journal of Nanomaterials and Biostructures* **8**, 1590 (2014).

- [20] T.S. Sreeprasad, S.M. Maliyekkal, K.P. Lisha, T. Pradeep, *J Hazard Mater* **186**, 921 (2011).
- [21] G. Wang, X. Shen, B. Wang, J. Yao, J. Park, *Carbon* **47**, 1359 (2009).
- [22] A.S. Kochnev, I.A. Ovid'ko, B.N. Semenov, *Reviews on Advanced Materials Science* **37**, 105 (2014).
- [23] L. Fu, A. Wang, Y. Zheng, W. Cai, Z. Fu, *Materials Letters* **142**, 119 (2015).
- [24] S. Park, J. An, R.D. Piner, I. Jung, D. Yang, A. Velamakanni, S.T. Nguyen, R.S. Ruoff, *Chemistry of Materials* **20**, 6592 (2008).
- [25] W.S. Hummers, R.E. Offeman, *Journal of the American Chemical Society* **80**, 1339 (1958).
- [26] J.I. Paredes, S. Villar-Rodil, A. Martínez-Alonso, J.M.D. Tascón, *Langmuir* **24**, 10560 (2008).
- [27] Z. Liu, J.T. Robinson, X. Sun, H. Dai, *Journal of the American Chemical Society* **130**, 10876 (2008).
- [28] Z.Y.-L.F.H.-F.X.I.A.W.Z.W.-Q.W.M.-Z. Zuo Ping-Ping, *Chemical Journal of Chinese Universities* **34**, 692 (2013).
- [29] W.C.-J. SUN Yu-Jiao, GENG Teng-Fei, WANG Zhong-Fu, HUANG Lin-Juan, *Acta Chimica Sinica* **69**, 1697 (2011).
- [30] K. Ganesan, L. Ratke, *Soft Matter* **10**, 3218 (2014).
- [31] S. Hashemian, M. Reza Shahedi, *Journal of Chemistry* **2013**, 7 (2013).
- [32] W. Li, C. Sun, B. Hou, X. Zhou, *International Journal of Spectroscopy* **2012**, (2012).
- [33] L. Xiong, Y. Yang, J. Mai, W. Sun, C. Zhang, D. Wei, Q. Chen, J. Ni, *Chemical Engineering Journal* **156**, 313 (2010).
- [34] D. Kavitha, C. Namasivayam, *Bioresource Technology* **98**, 14 (2007).
- [35] M. Ghaedi, E. Nazari, R. Sahraie, M.K. Purkait, *Desalination and Water Treatment* **52**, 5504 (2013).
- [36] K.Y. Foo, B.H. Hameed, *Chemical Engineering Journal* **156**, 2 (2010).
- [37] O. Abdelwahab, *Desalination* **222**, 357 (2008).
- [38] C. Ng, J.N. Lasso, W.E. Marshall, R.M. Rao, *Bioresource Technology* **85**, 131 (2002).